Linear formation-flying astronomical interferometry in low-Earth orbit: a feasibility study

Hansen, Jonah, Ireland, Michael, Travouillon, Tony, Lagadec, Tiphaine, Mathew, Joice, et al.

Jonah T. Hansen, Michael J. Ireland, Tony Travouillon, Tiphaine Lagadec, Joice Mathew, Nicholas Herrald, "Linear formation-flying astronomical interferometry in low-Earth orbit: a feasibility study," Proc. SPIE 11443, Space Telescopes and Instrumentation 2020: Optical, Infrared, and Millimeter Wave, 1144366 (13 December 2020); doi: 10.1117/12.2560890

Event: SPIE Astronomical Telescopes + Instrumentation, 2020, Online Only

Linear formation-flying astronomical interferometry in low-earth orbit: A feasibility study

Jonah T. Hansen[a], Michael J. Ireland[a], Tony Travouillon[a], Tiphaine Lagadec[a], Joice Mathew[a], and Nick Herrald[a]

[a]Research School of Astronomy & Astrophysics, Australian National University, ACT 2611, Australia

ABSTRACT

Space interferometry is the inevitable endpoint of high angular resolution astrophysics, and a key technology that can be leveraged to analyse exoplanet formation and atmospheres with exceptional detail. Here, we present a feasibility study into a small scale formation flying interferometric array, flying in Low Earth Orbit, that will aim to prove the technical concepts involved with space interferometry while still making unique astrophysical measurements. We will detail the design of the mission, as well as present orbital simulations that show that the array should be stable enough to perform interferometry with <50 m/s/year Δv and one thruster per spacecraft. We also conduct observability simulations to identify what parts of the sky are visible for a given orbital configuration. We conclude with optimism that this design is achievable, and briefly discuss *Pyxis* - a ground testbed for this technology and the next step to demonstrate full mission feasibility.

Keywords: Space Interferometry, Formation-Flight, Exoplanets, CubeSats, Low Earth Orbit, Orbital Dynamics, Observability

1. INTRODUCTION

The study of exoplanets is arguably one of the biggest subfields in astronomy in current times. The first detection of 51 Peg b by Mayor and Queloz[1] and subsequent detections by *Kepler*[2] and other surveys have ignited the imaginations of researchers and their desires to know more about these alien worlds. However, there are a number of problems in studying planets, in particular when the objective is to capture a spectrum of an exoplanet's atmosphere to determine more about its formation, or to determine whether life exists on the surface. Currently, transmission spectroscopy is the main method for obtaining spectra from exoplanet atmospheres; but is very challenging for terrestrial atmospheres.[3]

Imaging a planet directly would be the best approach, where one can get spectra through traditional methods, but separating the light of an exoplanet from a star is difficult due to two main obstacles. The first is due to contrast: the contrast between the star and a 300 K terrestrial planet (using the Sun/Earth ratio as an analogue) is an astounding 10^{10} in visible light. We can reduce this by three orders of magnitude by looking in the mid-infrared,[4] but we then encounter the issue that the Earth's atmosphere is opaque at these wavelengths, and ground based telescopes will give off substantial thermal background. Hence, a mid-infrared space based telescope is the ideal solution to achieve zodiacal-limited observations.

The second concern is that of angular resolution: for a planet 1 AU out from a host star at 10 pc, a minimum angular resolution of 0.1 arcsec would be required to distinguish the planet from the star. For a coronagraphic inner working angle of $2\lambda/D$ and a 15 micron wavelength, detecting such an exoplanet would require a 60m telescope. Such a sized telescope is incredibly difficult to construct on the ground, let alone send into space. To get around this, interferometry provides a tantalising solution as one can achieve high spatial resolution with small apertures due to large baselines.

Hence, if we want to conquer both of these concerns at once, we should combine both solutions: a space-based mid-infrared interferometer. Such a telescope would be complementary to an optical/near-infrared coronagraph

Send correspondence to Jonah Hansen - E-mail jonah.hansen@anu.edu.au

Space Telescopes and Instrumentation 2020: Optical, Infrared, and Millimeter Wave, edited by Makenzie Lystrup, Marshall D. Perrin, Proc. of SPIE Vol. 11443, 1144366 · © 2020 SPIE
CCC code: 0277-786X/20/$21 · doi: 10.1117/12.2560890

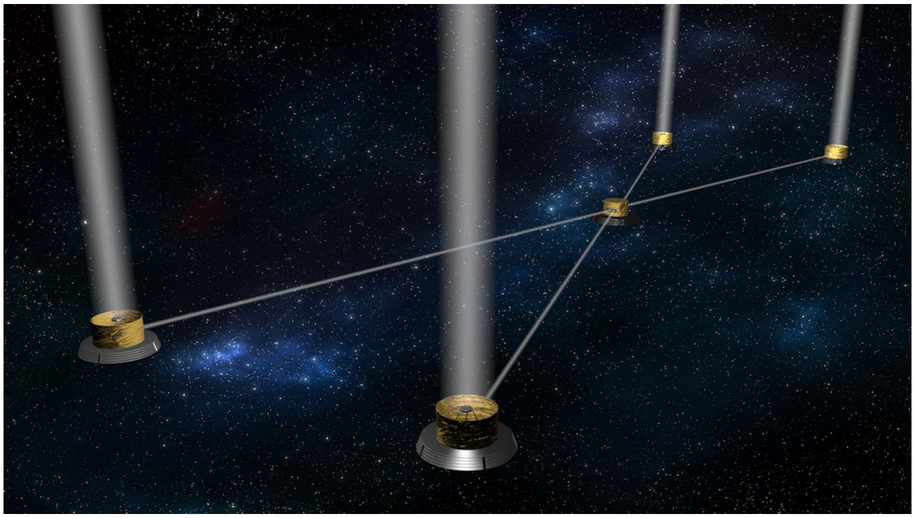

Figure 1: Artists interpretation of the LIFE mission.[14] Although the final configuration may look quite different (e.g. an Emma X-array), the general principles and the utility of a pathfinder remain.

space telescope, we find that it would detect more planets around cool stars in particular.[5] This is significant as the costs for a large scale space-based mid-infrared interferometric mission (such as *Darwin*) would be more economical (∼\$1.2B[6]) than the equivalent space-based optical telescope (e.g. LUVOIR at > \$10B[7]).

2. MOTIVATION FOR A TECHNOLOGY PATHFINDER

The first design of a space-based interferometer for the purpose of exoplanet research was proposed by Bracewell,[8] and then studied extensively in the 1980s and 90s by the European Space Agency (ESA) as part of their Horizon 2000 plan.[9] These studies led to the development of two flagship missions: NASA's Terrestrial Planet Finder Interferometer (TPF-I) mission[10] and ESA's *Darwin* mission.[11] Both of these missions were free flying arrays of satellites orbiting around the Sun-Earth L2 point in a configuration known as the "Emma X-array', an arrangement consisting of the four telescopes flying in rectangular formation and the beam combiner located about 1200 m above the array.[12] Unfortunately, due to budget cuts and the lack of technology readiness in the mid 2000s, both of these concepts did not progress beyond the design study.

Since then, there has been limited developments on the space interferometry front, but very recently there has been a renewal of interest in the field. As part of the discussion for ESA's Voyage 2050 plan, a *Darwin*-like mission called *LIFE* (Large Interferometer For Exoplanets) has been proposed.[5,13] An artist's impression of such a mission is shown in Figure 1. To approach technological readiness for such a mission, smaller pathfinder studies must be undertaken. One of the more critical of these is formation flying interferometry - keeping multiple satellites in formation at the required stability level to perform interferometry.

We have hence proposed a pathway for developingt technological readiness for formation flying space interferometry, shown in Figure 2. First is a ground pathfinder, named *Pyxis*, using robots in the carpark of Mt Stromlo Observatory in Canberra to identify whether the formation flying control system, including metrology (knowing the relative locations of the satellites) will be sufficiently stable for interferometry. The understanding from this prototype can then be put into developing a CubeSat mission, hereby known as *ASP* (Astrophysical Space-Interferometry Pathfinder), for which this paper mainly concerns. After this point, another larger scale mission could be studied, namely a space-based version of the Planet Formation Imager.[15] This would act as a final stepping stone between technology demonstration and the final *LIFE* mission.

The rest of this paper will detail a feasibility study we conducted into *ASP* and formation flying interferometry, before summarising current developments in this space.

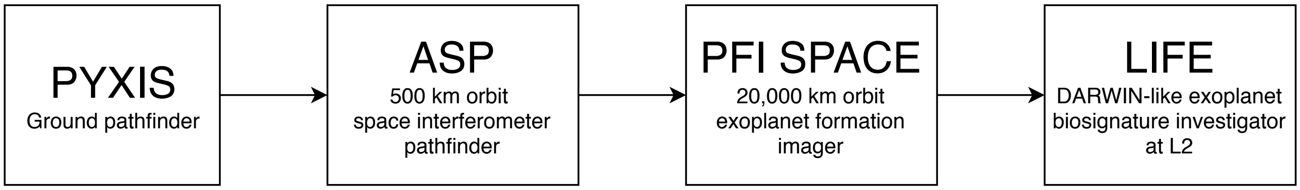

Figure 2: Proposed pathway towards a full scale space interferometry mission such as *LIFE*. *Pyxis* is currently being explored at the Australian National University. This paper concerns *ASP*, a CubeSat pathfinder.

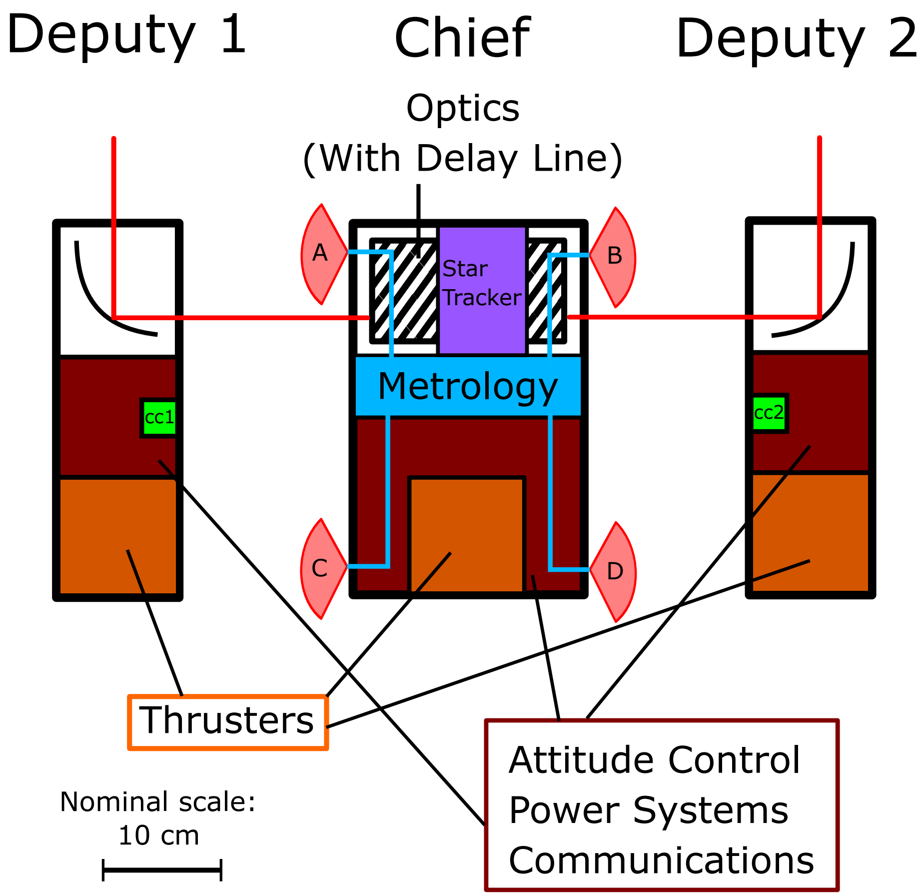

Figure 3: Schematic of the architecture for the Astrophysical Space-interferometer Pathfinder *ASP*.[16] The deputies are nominally 3U CubeSat, off-axis paraboloidal telescopes. The chief, a 6U CubeSat, acts as the beam combiner and controller of the array, containing the star tracker, beam combination optics and metrology system. The metrology is explored more in poster 11446-33 of session P4 (Lagadec, 2020).

3. SYSTEM ARCHITECTURE

Our proposed design consists of three CubeSats flying in a linear array. Two of the satellites, known as the deputies, are 3U in size and act as telescopes in collecting the light from the target and directing it to the beam combiner. The beam combiner, known as the chief, sits in the centre of the array and is 6U in size. A diagram of the design is shown in Figure 3.

As seen in the diagram, each satellite has a single thruster due to space constrains. We will show later on that this should still be sufficient in maintaining formation throughout the orbit. The mission is proposed to fly at an altitude of 500 km and have a lifetime of three years.

Fundamental to interferometery, we need to ensure that the optical path length between the two arms of the interferometer are identical. That is, the optical path difference should be as close to zero as we can make it. We can write the optical path difference with the following equation:

$$\Lambda = |\Delta \boldsymbol{r}_1| - \Delta \boldsymbol{r}_1 \cdot \hat{\boldsymbol{s}} - |\Delta \boldsymbol{r}_2| + \Delta \boldsymbol{r}_2 \cdot \hat{\boldsymbol{s}} \approx 0, \tag{1}$$

where $\Delta \boldsymbol{r}$ is the separation of one of the deputies from the chief, and $\hat{\boldsymbol{s}}$ is the unit vector in the direction of the star/target. To maintain this constraint, we need to have very precise knowledge on the separations of the satellites in order to counteract any residual difference. This metrology system is one of the key technologies we are testing with the *Pyxis* project, and is explained more in detail by poster 11446-33 of session P4 (Lagadec, 2020).

Target acquisition will be provided by a star tracker on the chief spacecraft. The JPL Astera CubeSat demonstrated 0.5 arcsecond pointing accuracy with 1 milliarcsecond repeatability;[17] we hope that we will be able to leverage a similar design to ensure similarly accurate pointing. Once the target is acquired by the chief, it will relay attitude and orbital adjustments to the deputies, which then allow the array to begin measurements of the target. The two telescopes being considered for the deputies are diamond turned off-axis paraboloids, manufactured out of aluminium. The advantages of using diamond-turned aluminium optics include reducing the impact of thermal expansion, the ability to make the telescope light, and being cost effective when compared to using precision glass optics. The light from the off-axis paraboloid is directed out of the telescope satellite, towards the beam combiner. The injection and beam combiner architecture will be briefly explored in the later Section 6.

Considering the 6U + 3U + 3U array design, we foresee the array being launched as one 12U payload. Each satellite will require five actuators for deployment: two to separate from the combined payload, and three for solar panel deployment. The solar panel actuators will have to be active during observations, to act as baffles against solar light contamination.

4. ORBITAL DYNAMICS

The key focus of a formation flying interferometer feasibility study is looking at the orbital dynamics of such a mission. As mentioned previously, for an interferometer to function, we need all telescopes pointing towards the target with minimal optical path difference (Equation 1). To make this easier, we can try and ensure that the orbit is configured in such a way that the array is always perpendicular to the incoming light. In other words, the baseline of the interferometer is orthogonal to $\hat{\boldsymbol{s}}$.

This highlights why a formation flying array is ideal: a fixed array would require a large amount of thrust and orbit keeping to maintain orthogonality, particularly in the presence of tidal accelerations. These accelerations are of order $\mu r^{-3}|\Delta \boldsymbol{r}| = \omega^2 |\Delta \boldsymbol{r}|$, with ω the angular velocity of the orbit, μ the Earth's standard gravitational parameter, r the orbital radius and $|\Delta \boldsymbol{r}|$ the satellite separation. For a 500 km orbit and 300 m spacecraft separation, this is $0.4\,\mathrm{mm\,s^{-2}}$; beyond typical accelerations from plasma thrusters.

Returning to the formation flying concept, having the baseline always perpendicular to the target reduces the complexity of maintaining the optical path: only perturbations in the direction of the target and those along the baseline need to be considered. We can mathematically derive such a configuration as follows. We will refer to the orbit of the chief satellite as the reference orbit.

We have the freedom to configure the reference orbit in any orbital plane we desire; based on launch, target and external factors. Let's call the reference orbit inclination i and the longitude of the ascending node Ω. For a given reference orbit, there is a single configuration for the two deputies such that the orthogonality requirement, $\Delta \boldsymbol{r}(t) \cdot \hat{\boldsymbol{s}} = 0$, is satisfied for all t. We now consider the local vertical, local horizontal (LVLH) reference frame for the following analysis. This is a rotating curvilinear reference frame that is centred on the chief satellite's motion. The frame's unit vectors are defined as $\hat{\boldsymbol{\rho}}$ being along the radial position of the chief satellite, $\hat{\boldsymbol{\xi}}$ pointing in the along-track direction (velocity) of the chief satellite and $\hat{\boldsymbol{\eta}}$ pointing in the cross-track (angular momentum) of the chief satellite. Hence the reference orbital plane is equivalent to the $\hat{\boldsymbol{\rho}} - \hat{\boldsymbol{\xi}}$ plane. A schematic of the LVLH frame is shown in Figure 4

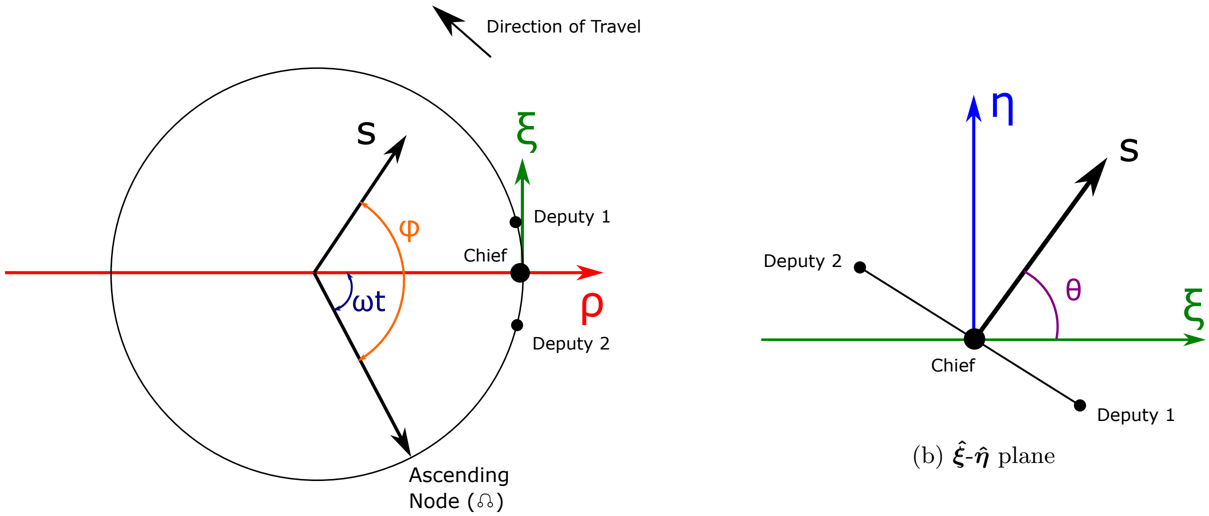

(a) $\hat{\boldsymbol{\rho}}$-$\hat{\boldsymbol{\xi}}$ plane

(b) $\hat{\boldsymbol{\xi}}$-$\hat{\boldsymbol{\eta}}$ plane

Figure 4: Schematic of the LVLH frame, including the target vector angles θ and ϕ.[16]

We now consider the target vector in this frame, having spherical coordinates (θ,ϕ) being the polar angle and azimuthal angle from the ascending node of the orbital plane (☊) respectively. These two angles can be formed from the orbital parameters of the reference orbit given the right ascension (α) and declination (δ) of the target:

$$\cos(\theta) = \sin(\delta)\cos(i) - \cos(\delta)\sin(i)\sin(\alpha - \Omega)$$
$$\sin(\phi) = \frac{\cos(\delta)\cos(i)\sin(\alpha - \Omega) + \sin(\delta)\sin(i)}{\sin(\theta)}$$
$$\cos(\phi) = \frac{\cos(\delta)\cos(\alpha - \Omega)}{\sin(\theta)}$$

.

Finally, we consider that the chief satellite has a phase ωt from the ascending note of the orbit. In the LVLH frame, the target vector with respect to the chief satellite becomes:

$$\hat{\boldsymbol{s}} = [\cos(\phi - \omega t)\sin(\theta), \sin(\phi - \omega t)\sin(\theta), \cos(\theta)]. \tag{2}$$

We can now analyse the motion of the array in this reference frame, to identify what formation the two deputies can fly in with respect to the chief. To do this, we use the HCW equations of motion for the LVLH frame,[18] which assume a circular orbit with no perturbations:

$$\ddot{\rho} = 3\omega^2\rho + 2\omega\dot{\xi} \tag{3}$$
$$\ddot{\xi} = -2\omega\dot{\rho} \tag{4}$$
$$\ddot{\eta} = -2\omega^2\eta. \tag{5}$$

These equations can be solved yielding the position of a deputy satellite $\Delta\boldsymbol{r}(t) = [\rho(t), \xi(t), \eta(t)]$, where

$$\rho(t) = \kappa_1 + \kappa_2\cos(\omega t - \kappa_3) \tag{6}$$
$$\xi(t) = \kappa_4 - \frac{3\omega}{2}\kappa_1 t - 2\kappa_2\sin(\omega t - \kappa_3) \tag{7}$$
$$\eta(t) = \kappa_5\cos(\omega t) + \kappa_6\sin(\omega t) \tag{8}$$

and κ_1 through κ_6 are constants found through the initial conditions.

We see immediately some constraints on the initial conditions that have to be made in order for the formation to remain stable. In equation 7, if $\kappa_1 \neq 0$, the angular momentum will not be conserved and the spacecraft will fly apart. We can also make a judicious choice of initial conditions such that κ_2 is zero. The orthogonality constraint then becomes:

$$\begin{aligned}\Delta \boldsymbol{r}(t) \cdot \hat{\boldsymbol{s}} =& \kappa_4(\cos(\omega t)\sin(\phi) - \sin(\omega t)\cos(\phi))\sin(\theta) \\ &+ \kappa_5\cos(\omega t)\cos(\theta) + \kappa_6\sin(\omega t)\cos(\theta).\end{aligned} \tag{9}$$

Finally, if we set initial conditions such that

$$\kappa_5 = -\kappa_2\tan(\theta)\sin(\phi) \qquad \kappa_6 = \kappa_2\tan(\theta)\cos(\phi), \tag{10}$$

we ensure the orthogonality constraint holds for all t.

Finally, the equations of motion under these initial positions then become:

$$\rho(t) = 0 \tag{11}$$

$$\xi(t) = \kappa_4 \tag{12}$$

$$\eta(t) = -\kappa_4\tan(\theta)\sin(\phi - \omega t) \tag{13}$$

This gives us the solution we were looking for: a linear array of satellites will indeed work. In this configuration, the deputy satellites will move up and down in the $\hat{\boldsymbol{\eta}}$ direction with a period equal to that of the orbital period, and with an offset in the $\hat{\boldsymbol{\xi}}$ direction. Converting backwards into orbital elements, this indicates that a configuration where the deputies have a slight inclination/longitude offset from the reference orbit will suffice in keeping the array perpendicular to the target at all times.

5. COUNTERACTING PERTURBATIONS

Unfortunately, the discussion previous assumed orbits in the absence of perturbations. At an altitude of 500 km, There are a number of perturbations to consider and correct; in particular the J_2 gravitational perturbation due to the Earth's oblateness, and atmosperic drag.

We remind the reader here that we only need to consider perturbations along the baseline, and in the direction of the target. Any perturbations orthogonal to these directions will not affect the optical path difference and so don't need to be actively corrected during integration. After orbital simulations were performed, we found that over the course of half an orbit the J_2 gravitational perturbation would affect the satellites on the order of 1 m in the target direction at 500 km. The perturbation did not seem to affect the motion in the baseline direction much at all.

For atmospheric drag, the effect will be in the baseline direction with the chief satellite moving closer to one of the deputies than the other. Assuming an acceleration on the order of 1×10^{-7} ms^{-}2 at 500 km, the displacement over half an orbit would be on the order of 35 cm.

As drag would shorten one path and lengthen the other, and as we only have one thruster (nominally in the direction of the target), we can fix the perturbation by thrusting one of the deputies up by about twice the displacement (as shown in Figure 5). Over a separation between the chief and deputy of 300m, the required displacement is small enough to keep the deputy within the field of view of the chief.

After identifying the main perturbations, we then calculated what it would take to correct them. We separated corrections into three categories: active correction during the observation, correcting the orbit during the half of the orbit that the array is recharging in sunlight, and re-configuring the orbit for a different target or baseline. We quantified this using the Δv parameter; the change in velocity due to an impulsive manoeuvre.[19] The spacecraft array will have a Δv budget, the total change in velocity that can be made over the lifetime of the mission, and can be used as a stand in for the amount of fuel required.

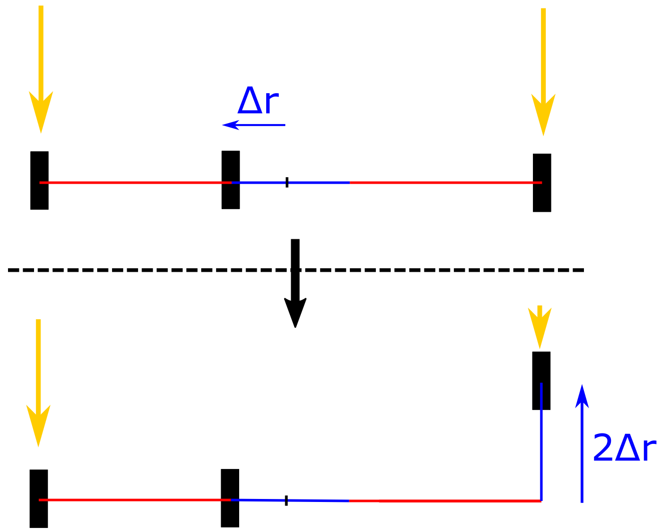

Figure 5: Schematic illustrating the correction of a displacement in the baseline direction by thrusting towards the target.[16]

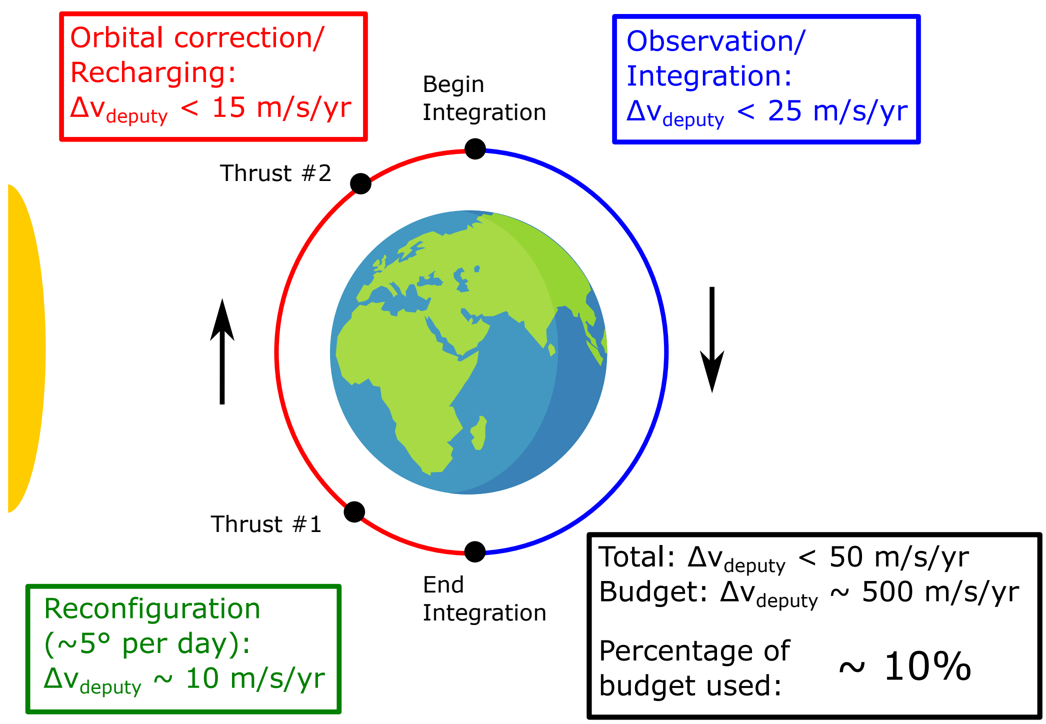

Figure 6: Schematic of the Δv required to counteract perturbations during various portions of an orbit.[16]

We took an example thruster, the Enpulsion Spacecraft Technology thruster[20]m which has a total budget of 5000 Ns. This translates into $\Delta v \approx 2$km/s for a 3 kg 3U CubeSat and $\Delta v \approx 1$km/s for the larger 6U CubeSat. The Δv requirements for the different corrections, based on orbital simulations, are summarised in Figure 6 for a deputy satellite over a 3 year mission.

The blue part of the diagram indicates the active correction during an observation. This occurs for half an orbit, while the array is on the nighttime side of the Earth. We numerically calculated the displacement in the baseline and target directions due to both J_2 and atmospheric drag, and find that it would take on the order of 25 m/s/yr of Δv to counteract them.

The red section of the diagram represents the other half of the orbit, when the array is recharging in the sunlight. Here, we assume that the array drifts except for two intentional thrusts 10 minutes after the observation, and 10 minutes before it restarts observing. These thrusts are designed to manoeuvre the array into a position as close to the beginning of the orbit as possible.

As these two thrusts can be in any direction, we have six free variables. The final end state vector also has six parameters (three position and three velocity), and so the two thrusts give us the ability to move into any state vector we require. Numerically solving the orbits to bring the array back into position gives us a Δv requirement of 15 m/s/yr.

Finally, the green segment considers the Δv required to reconfigure the orbit based on a change of baseline or target. Assuming a slew rate of $\tilde{5}^{\circ}$per day, this requires a Δv of 10 m/s/yr.

Combining these results, we identify that a deputy satellite would use 50 m/s/yr, or 10% of the budget. This indicates that one thruster is indeed enough for our purposes, and has headroom for other manoeuvres due to the control system or emergencies.

6. INJECTION AND BEAM COMBINATION

On the Chief spacecraft, other than the boresight star tracker, the key optics will be the alignment camera including pupil and fiber injection, as well as the science and metrology beam combiners. Both the science and metrology beam combiners are expected to be based on photonic chips, with overall volumes of approximately 100 x 50 x 50mm each.

The alignment and injection optics, which has to include optical delay, might be considered challenging to fit into a small volume. An initial concept is shown in Figure 7, where both pupil and image alignment on both beams are measured on a single camera. This concept, to be prototyped as part of *Pyxis* in 2021, includes different elements for science wavelengths (∼600-800 nm) and the the two polarisations of the alignment wavelengths (∼400-600 nm). The science wavelengths follow a simple path: microscope tube lens, collimator, transmission through a dichroic and then fiber injection via a translation stage acting as the delay line. The alignment wavelengths reflect off the dichroic and knife-edge mirror before being split in polarisation, enabling simultaneous pupil and image detection for beams of both satellites on a 1x1mm sensor. The collimator lens is translatable by piezoelectric transducers for angular alignment. Alignment of the incoming pupil is achieved via a pointing offset to the deputy spacecraft.

The beam combiner will be a photonic chip in the form of a "tricoupler", a set of three waveguides in a three dimensional triangular layout that will split the light with a phase offset of $\pm\frac{2\pi}{3}$. This allows us to fully recover the complex visibility for a given baseline, while keeping the structure relatively simple and maximising throughput. We aim to conduct spectropolarimetry with such a device, and so a photonic chip will reduce the complexity involved in maintaining a polarisation state. As with the injection optics, we aim to prototype these as a part of *Pyxis* in 2021.

7. OBSERVABILITY

Apart from the orbital dynamics, we also considered what part of the sky this array would be able to view over a year. Two particular issues were identified that would prevent a measurement from taking place.

The first was the presence of the Sun. Both the beam path and the telescope must be in shadow during observation, else risking likely solar contamination. We quantified this using the antisolar angle γ - the largest

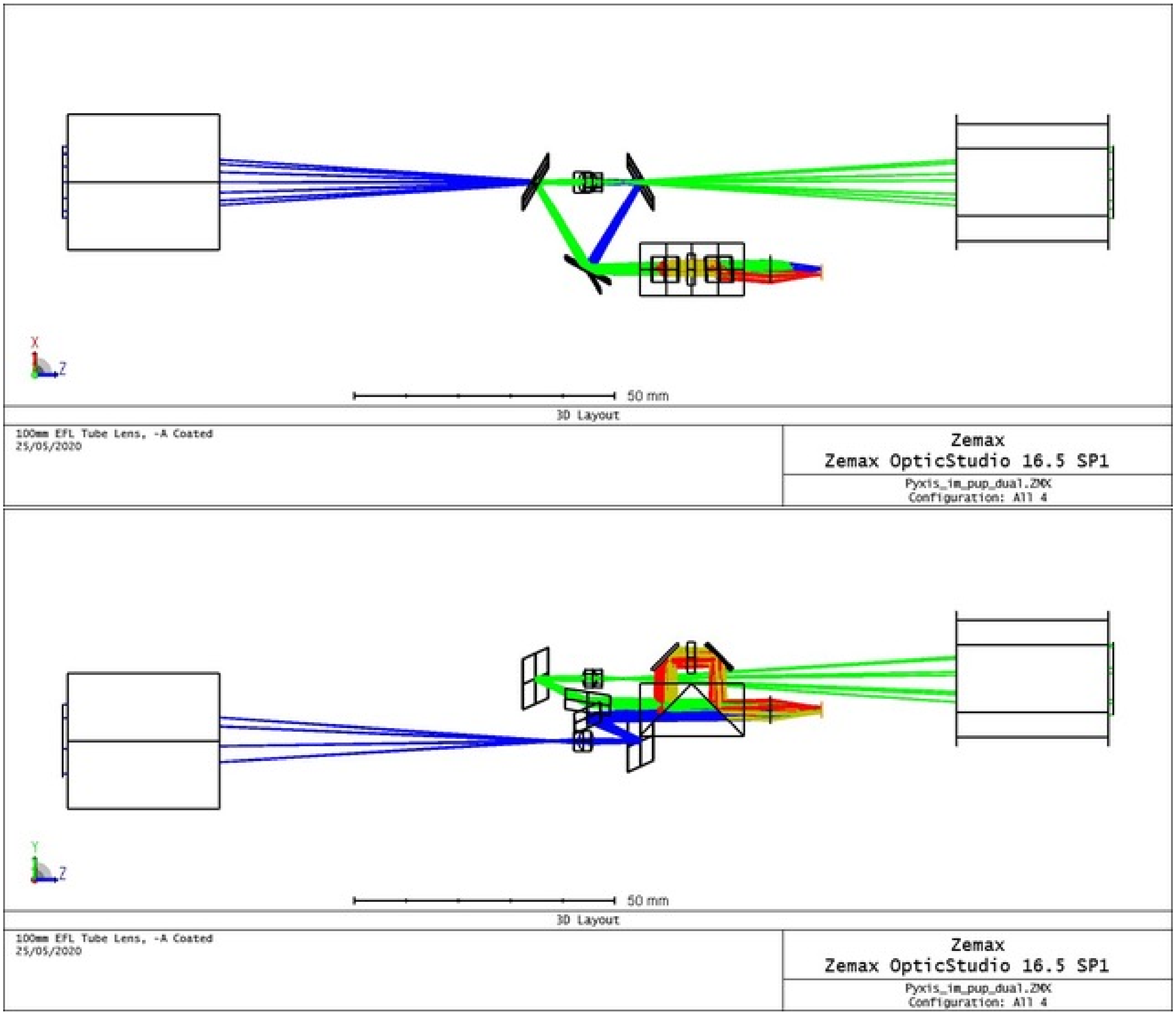

Figure 7: Layout of an initial design for injection. Top: Side-on view. Bottom: Near top-down view. Collimated beams from the two deputies come from the right and the left of the images. Not shown are the ∼2mm diameter collimated beams travelling through the dichroics (first angled mirror in the top-down view) and on to the a ∼1cm travel piston translator to the science fiber injection.

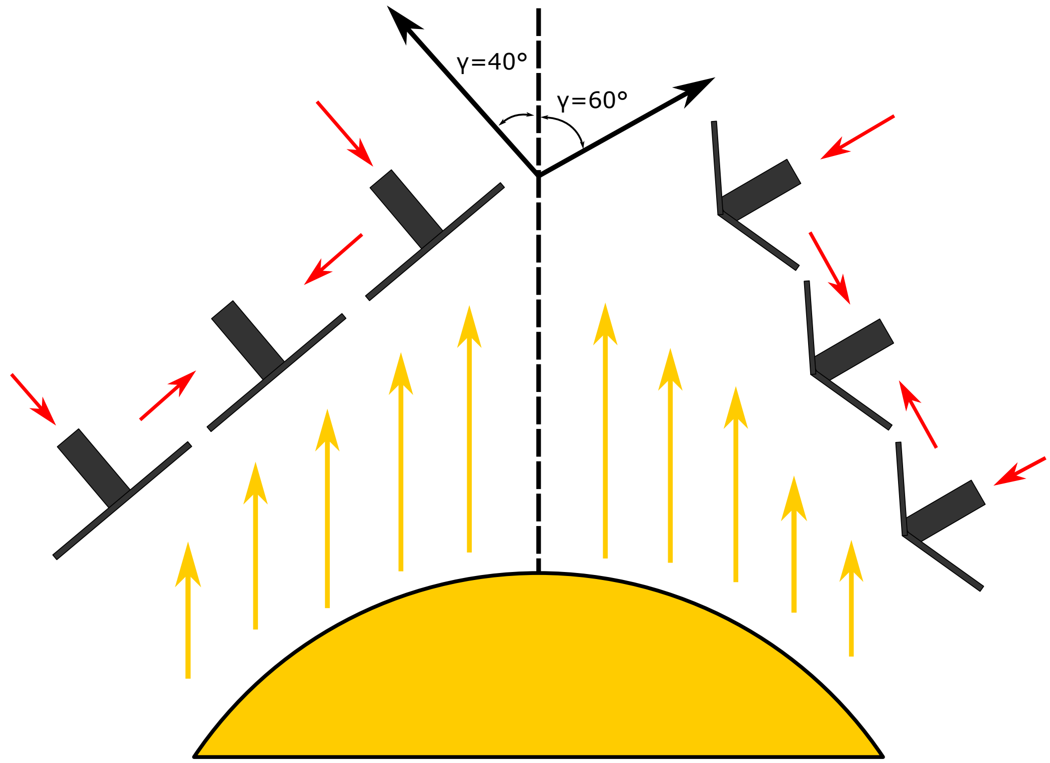

Figure 8: Schematic showing the concept of the antisolar angle - the maximum angle the array can make with the antisolar axis before the Sun interferes with a measurement.[16] At 60°, the solar panels, acting as baffles, will need to fold inwards to prevent Solar contamination.

angle that the target vector can make with the antisolar axis. An example of this concept is shown in Figure 8. We note that while we want to increase this angle to be as large as possible for maximum sky coverage, 60°is likely the largest we can achieve with easily deployable baffling.

The second issue is whether the Earth blocks an observation. To account for the fact that the Earth glows, we extended the radius of the Earth slightly when simulating when the Earth obscures the target. Light from the Earth contaminating the beam path was able to be ignored as the baseline should always be tangential to the surface of the Earth. Other potential issues were deemed less important, such as the obscuration and reflectivity of the Moon.

We ran a simulation of what portion of the sky is viewable over a year's worth of orbits. A map of the sky for two different configurations in ecliptic coordinates is found in Figure 9. Figure 9a depicts a heliosynchronous orbit with a longitude of 90°from the vernal equinox. This orbit is common for LEO satellites, and allows targets at opposition from the sun to be viewed over a complete orbit, rather than the half an orbit assumed in Figure 6. This results in the bright stripe seen at low Ecliptic latitudes. Due to the recharging requirement though, observation times should still be kept at 45 minutes (half an orbit at 500 km. The second plot (Figure 9b) has an inclination of 39°- the lowest inclination that the rocket company Rocket Lab can achieve.[21] This was chosen due to the proximity to the assembly location (Australia), and so likely being the least expensive custom launch option.

The main insight from these plots can be seen in that the antisolar angle sets the ecliptic latitude at which a target may be viewable; a target with a latitude larger than the antisolar angle cannot be viewed at all. We also see that targets with latitudes $-40° < \beta < 40°$ are viewable for between 15 and 25% of the year.

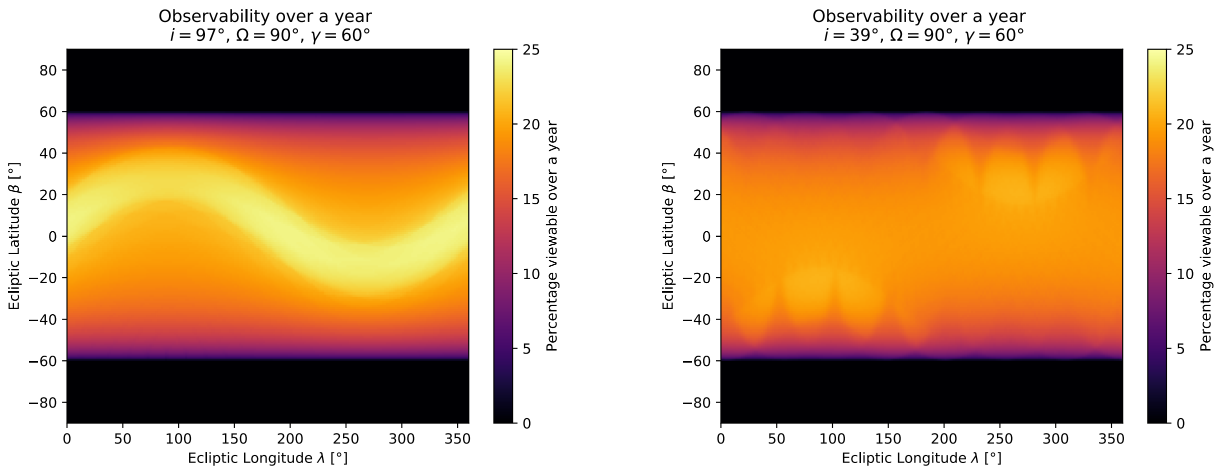

(a) Longitude $\Omega = 90^\circ$, Inclination $i = 97^\circ$

(b) Longitude $\Omega = 90^\circ$, Inclination $i = 39^\circ$

Figure 9: Map of the satellite sky coverage for different orbital configurations, as a percentage observable over a year, shown in ecliptic coordinates.[16] The antisolar angle was set at 60° for both plots.

8. CONCLUSIONS AND FUTURE DEVELOPMENTS

This feasibility study has shown that a Low Earth Orbit CubeSat mission such as *ASP* should be feasible in performing interferometry on a number of targets, and that the Δv budget for a single thruster should be sufficient in counteracting the necessary perturbations while allowing room for slewing and reconfiguration. The biggest question that remains concerns the metrology system and a practical test of the formation flying control system.

To this end, we have started developing a ground prototype of the array named *Pyxis*. This is a prototype made of three robots in the carpark of Mt Stromlo Observatory, who will act as the CubeSats described in this paper. In the development of *Pyxis*, we will also formalise the interferometric metrology for the formation flying control system. We aim to test many of the subsystems for the full CubeSat mission, with the exception of the satellites themselves. *Pyxis* will also conduct it's own scientific research into red giants using interferometric polarimetry, with aims for on-sky observations starting 2023. We then hope that hardware development of *ASP* can start in earnest with a launch in the years following.

ACKNOWLEDGMENTS

This research was supported by the Australian Government through the Australian Research Council's Discovery Projects funding scheme (project DP200102383), and by the Australian National University through the Futures scheme.

REFERENCES

[1] Mayor, M. and Queloz, D., "A Jupiter-mass companion to a solar-type star," *Nature* **378**, 355–359 (11 1995).

[2] Borucki, W. J., Koch, D., Basri, G., Batalha, N., Brown, T., Caldwell, D., Caldwell, J., Christensen-Dalsgaard, J., Cochran, W. D., DeVore, E., Dunham, E. W., Dupree, A. K., Gautier, T. N., Geary, J. C., Gilliland, R., Gould, A., Howell, S. B., Jenkins, J. M., Kondo, Y., Latham, D. W., Marcy, G. W., Meibom, S., Kjeldsen, H., Lissauer, J. J., Monet, D. G., Morrison, D., Sasselov, D., Tarter, J., Boss, A., Brownlee, D., Owen, T., Buzasi, D., Charbonneau, D., Doyle, L., Fortney, J., Ford, E. B., Holman, M. J., Seager, S., Steffen, J. H., Welsh, W. F., Rowe, J., Anderson, H., Buchhave, L., Ciardi, D., Walkowicz, L., Sherry, W., Horch, E., Isaacson, H., Everett, M. E., Fischer, D., Torres, G., Johnson, J. A., Endl, M., MacQueen,

P., Bryson, S. T., Dotson, J., Haas, M., Kolodziejczak, J., Van Cleve, J., Chandrasekaran, H., Twicken, J. D., Quintana, E. V., Clarke, B. D., Allen, C., Li, J., Wu, H., Tenenbaum, P., Verner, E., Bruhweiler, F., Barnes, J., and Prsa, A., "Kepler Planet-Detection Mission: Introduction and First Results," *Science* **327**, 977 (Feb. 2010).

[3] Diamond-Lowe, H., Berta-Thompson, Z., Charbonneau, D., Dittmann, J., and Kempton, E. M. R., "Simultaneous Optical Transmission Spectroscopy of a Terrestrial, Habitable-Zone Exoplanet with Two Ground-Based Multi-Object Spectrographs," *arXiv e-prints* , arXiv:1909.09104 (Sep 2019).

[4] Angel, J. R. P. and Woolf, N. J., "An Imaging Nulling Interferometer to Study Extrasolar Planets," *The Astrophysical Journal* **475**, 373–379 (1 1997).

[5] Quanz, S. P., Kammerer, J., Defrère, D., Absil, O., Glauser, A., and Kitzmann, D., "Exoplanet science with a space-based mid-infrared nulling interferometer," in [*Optical and Infrared Interferometry and Imaging VI*], Mérand, A., Creech-Eakman, M. J., and Tuthill, P. G., eds., **10701**, 37, SPIE (7 2018).

[6] Cockell, C. S., Herbst, T., Léger, A., Absil, O., Beichman, C., Benz, W., Brack, A., Chazelas, B., Chelli, A., Cottin, H., Coudé du Foresto, V., Danchi, W., Defrère, D., den Herder, J.-W., Eiroa, C., Fridlund, M., Henning, T., Johnston, K., Kaltenegger, L., Labadie, L., Lammer, H., Launhardt, R., Lawson, P., Lay, O. P., Liseau, R., Martin, S. R., Mawet, D., Mourard, D., Moutou, C., Mugnier, L., Paresce, F., Quirrenbach, A., Rabbia, Y., Rottgering, H. J. A., Rouan, D., Santos, N., Selsis, F., Serabyn, E., Westall, F., White, G., Ollivier, M., and Bordé, P., "Darwin—an experimental astronomy mission to search for extrasolar planets," *Experimental Astronomy* **23**, 435–461 (3 2009).

[7] National Aeronautics and Space Administration, "LUVIOR final report," tech. rep., NASA (2019).

[8] Bracewell, R. N., "Detecting nonsolar planets by spinning infrared interferometer," *Nature* **274**, 780–781 (8 1978).

[9] Fridlund, C., "The search for exoplanets and space interferometry," *Planetary and Space Science* **50**, 101–121 (1 2002).

[10] Beichman, C. A., Woolf, N. J., and Lindensmith, C. A., "The Terrestrial Planet Finder (TPF) : a NASA Origins Program to search for habitable planets," tech. rep., Jet Propulsion Laboratory, California Institute of Technology, Pasadena, California (1999).

[11] Léger, A., Mariotti, J., Mennesson, B., Ollivier, M., Puget, J., Rouan, D., and Schneider, J., "Could We Search for Primitive Life on Extrasolar Planets in the Near Future?," *Icarus* **123**, 249–255 (10 1996).

[12] Defrère, D., Absil, O., and Beichman, C. A., "Interferometric Space Missions for Exoplanet Science: Legacy of Darwin/TPF," in [*Handbook of Exoplanets*], Hans J. Deeg and Juan Antonio Belmonte, eds., 1229–1255, Springer International Publishing, Cham (2018).

[13] Quanz, S. P., Absil, O., Angerhausen, D., Benz, W., Bonfils, X., Berger, J.-P., Brogi, M., Cabrera, J., Danchi, W. C., Defrère, D., van Dishoeck, E., Ehrenreich, D., Ertel, S., Fortney, J., Gaudi, S., Girard, J., Glauser, A., Grenfell, J. L., Ireland, M., Janson, M., Kammerer, J., Kitzmann, D., Kraus, S., Krause, O., Labadie, L., Lacour, S., Lichtenberg, T., Line, M., Linz, H., Loicq, J., Mennesson, B., Meyer, M. R., Miguel, Y., Monnier, J., N'Diaye, M., Pallé, E., Queloz, D., Rauer, H., Ribas, I., Rugheimer, S., Selsis, F., Serabyn, G., Snellen, I., Sozzetti, A., Stapelfeldt, K. R., Triaud, A., Udry, S., and Wyatt, M., "Atmospheric characterization of terrestrial exoplanets in the mid-infrared: biosignatures, habitability & diversity," *arXiv e-prints* **1908**, arXiv:1908.01316 (Aug. 2019).

[14] LIFE Project, [*Life Mission Artist's Impression*], LIFE Project. https://www.life-space-mission.com/the-project/technology/, Accessed 14th Nov 2020.

[15] Monnier, J. D., Kraus, S., Ireland, M. J., Baron, F., Bayo, A., Berger, J.-P., Creech-Eakman, M., Dong, R., Duchêne, G., Espaillat, C., Haniff, C., Hönig, S., Isella, A., Juhasz, A., Labadie, L., Lacour, S., Leifer, S., Merand, A., Michael, E., Minardi, S., Mordasini, C., Mozurkewich, D., Olofsson, J., Paladini, C., Petrov, R., Pott, J.-U., Ridgway, S., Rinehart, S., Stassun, K., Surdej, J., Brummelaar, T. t., Turner, N., Tuthill, P., Vahala, K., van Belle, G., Vasisht, G., Wishnow, E., Young, J., and Zhu, Z., "The planet formation imager," *Experimental Astronomy* **46**, 517–529 (Dec. 2018).

[16] Hansen, J. T. and Ireland, M. J., "A linear formation-flying astronomical interferometer in low Earth orbit," *Publications of the Astronomical Society of Australia* **37**, e019 (May 2020).

[17] Smith, M., Donner, A., Knapp, M., Pong, C., Smith, C., Luu, J., Pasquale, P., and Campuzano, B., "On-orbit results and lessons learned from the asteria space telescope mission. aiaa," in [*USU Conference on Small Satellites*], (2018).

[18] Clohessy, W. and Wiltshire, R., "Terminal Guidance System for Satellite Rendezvous," *Journal of the Aerospace Sciences* **27**, 653–658 (9 1960).

[19] Curtis, H. D., [*Orbital Mechanics for Engineering Students*], Elsevier Science and Technology, Oxford, third ed. (2014).

[20] Enpulsion Spacecraft Technology, "IFM Nano Thruster," (2018).

[21] Rocket Lab, "Payload User's Guide," tech. rep., Rocket Lab (2019).